

IRTM 11- $\mu\text{m}$  channel brightness temperatures to also decrease in regions where low 20- $\mu\text{m}$  channel brightness temperatures are observed [7,8]. The maps also show new phenomena, the most striking of which is a clear tendency for the low-brightness temperature regions to occur at fixed geographic locations. During this season, the coldest low brightness temperatures appear to be concentrated in distinct regions, with spatial scales ranging from 50 to 300 km. There are approximately a dozen of these concentrations, with the largest centered near the location of the south residual polar cap. Other concentrations are located at Cavi Angusti, and close to the craters Main, South, Lau, and Dana. Broader, less-intense regions appear to be well correlated with the boundaries of the south polar layered deposits, and the Mountains of Mitchell. We have thus far detected no evidence for horizontal motion of any of these regions.

The fact that the low brightness temperature regions do not appear to move and are correlated with the locations of surface features suggests that they are not artifacts of the IRTM instrument or its viewing geometry, but the result of processes occurring on the surface or in the lower atmosphere. Presently, we do not know whether other low brightness temperature regions that have been observed during the southern winter or during the northern fall and winter exhibit similar spatial and temporal behavior. We intend to better understand the cause(s) and implications of these phenomena through modeling and further analysis of the Viking and Mariner 9 datasets.

**References:** [1] Kieffer H. H. et al. (1976) *Science*, 193, 780-786. [2] Kieffer H. H. et al. (1977) *JGR*, 82, 4249-4291. [3] Hess S. L. (1979) *JGR*, 84, 2969-2973. [4] Diteon R. and Kieffer H. H. (1979) *JGR*, 84, 8294-8300. [5] Warren S. G. et al. (1990) *JGR*, 95, 14717-14741. [6] Hunt G. E. (1980) *GRL*, 7, 481-484. [7] Paige D. A. (1985) Ph.D. thesis, California Institute of Technology. [8] Paige D. A. and Ingersoll A. P. (1985) *Science*, 228, 1160-1168. [9] Pollack J. B. et al. (1990) *JGR*, 94, 1447-1473.

533-91 ABS. 01 N94-33223

**NUMERICAL SIMULATION OF THERMALLY INDUCED NEAR-SURFACE FLOWS OVER MARTIAN TERRAIN.** T. R. Parish<sup>1</sup> and A. D. Howard<sup>2</sup>, <sup>1</sup>Department of Atmospheric Science, University of Wyoming, Laramie WY 82071, USA, <sup>2</sup>Department of Environmental Sciences, University of Virginia, Charlottesville VA 22903, USA.

**Introduction:** The near-surface martian wind and temperature regimes display striking similarities to terrestrial desert counterparts [1,2]. The diurnal radiative cycle is responsible for establishment of a pronounced thermal circulation in which downslope (katabatic) flows prevail during the nighttime hours and weak upslope (anabatic) conditions prevail during the daytime. The low-level wind regime appears to play an important role in modifying the surface of the polar regions [3]. Viking imagery of the north polar cap shows evidence of eolian characteristics such as dunes, frost streaks, and wind-scour features. The direction of the prevailing wind can in cases be inferred from the orientation of surface features such as frost streaks and ice grooves.

For the past several years a numerical modeling study has been in progress to examine the sensitivity of thermally induced surface winds on Mars to the patterns of solar insolation and longwave radiative. The model used is a comprehensive atmospheric me-

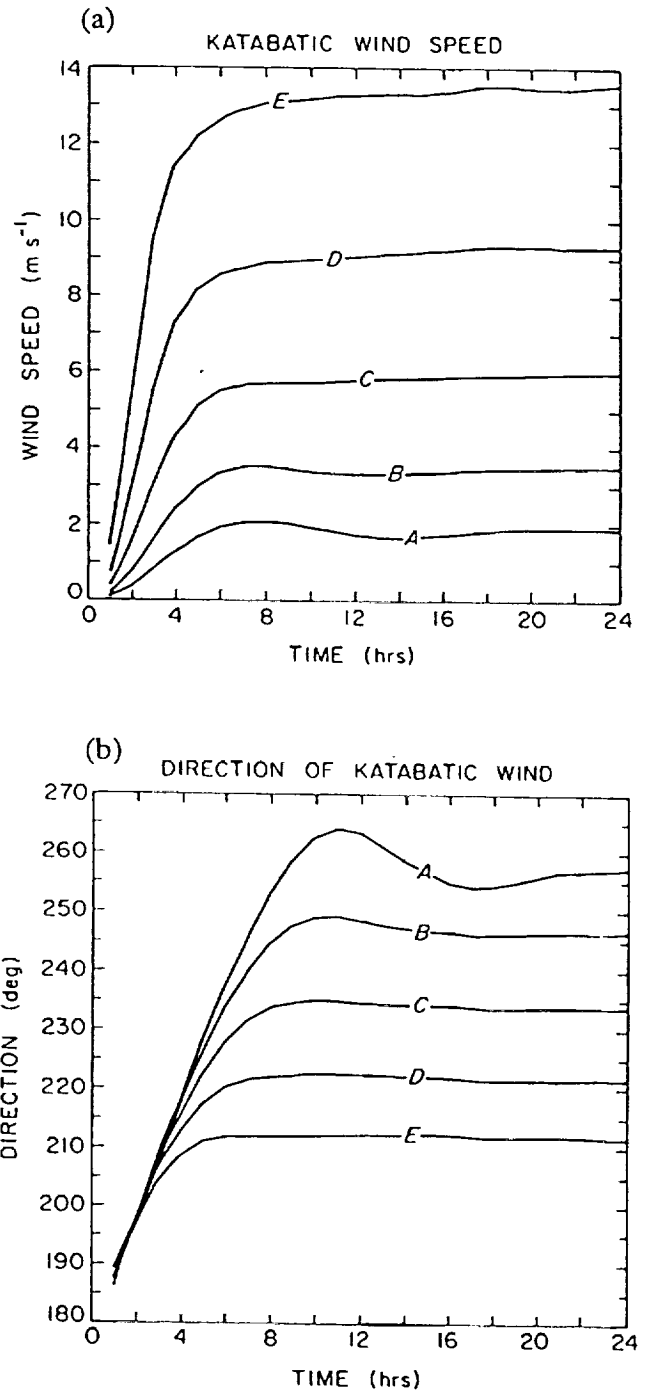
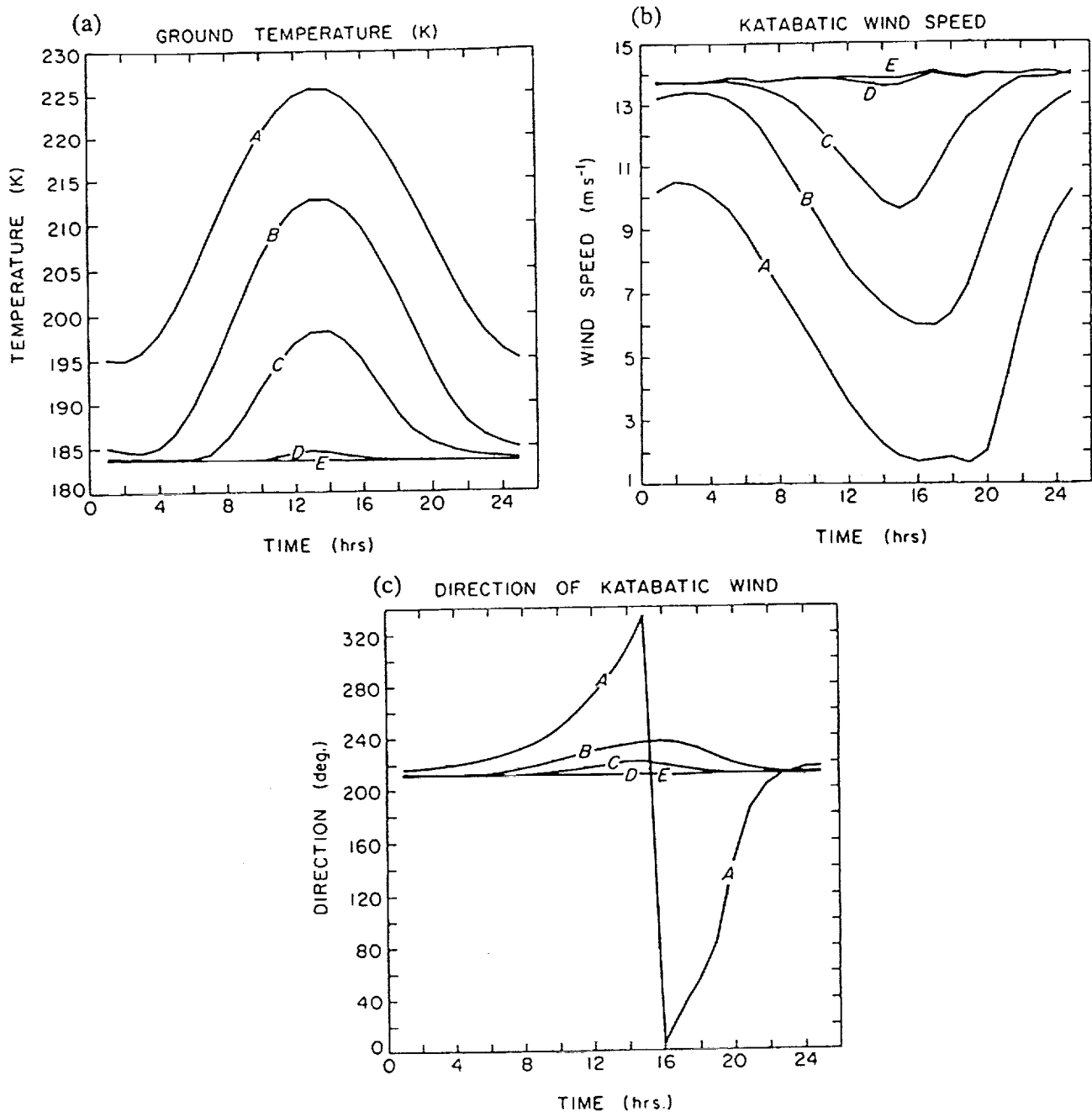


Fig. 1. Time evolution of (a) wind speed and (b) wind direction at the lowest sigma level (20 m) after 24-hr integration of constant slope runs for terrain slopes of 0.0005, 0.001, 0.002, 0.004, and 0.008, corresponding to curves A, B, C, D, and E respectively.

oscale equation system that has been employed previously for simulation of Antarctic katabatic winds [4]. The model equations are written in terrain-following sigma coordinates to allow for irregular terrain [5]; prognostic equations include the flux forms of



**Fig. 2.** Diurnal variation of (a) ground temperature, (b) wind speed, and (c) wind direction at the lowest sigma level for the solar cycle simulations over the 0.008 slope for solar declination angles of 24°, 12°, 0°, -12°, and -24°, corresponding to curves A, B, C, D, and E respectively.

the horizontal momentum equations, temperature, and continuity. A surface-energy budget equation is also incorporated in which the surface temperature is determined. Explicit parameterization of both solar insolation and longwave radiation is included. Turbulent transfer of heat and momentum in the martian atmosphere is assumed to follow the similarity expressions in the surface boundary layer on Earth [6-8]. The vertical grid consists of 15 levels ( $\sigma = 0.998, 0.99, 0.98, 0.97, 0.96, 0.94, 0.92, 0.90, 0.85, 0.775, 0.70,$

$0.60, 0.50, 0.30, 0.10$ ). The high resolution in the lower atmosphere is necessary to capture details of the boundary layer flows. The lowest level corresponds to a height of approximately 20 m above the ground, the second level to 100 m.

Probably the greatest uncertainty in model simulations of thermally driven martian flows is the specification of the terrain. While detailed topographic information is available for certain regions, only a fairly broadscale representation is possible over the martian

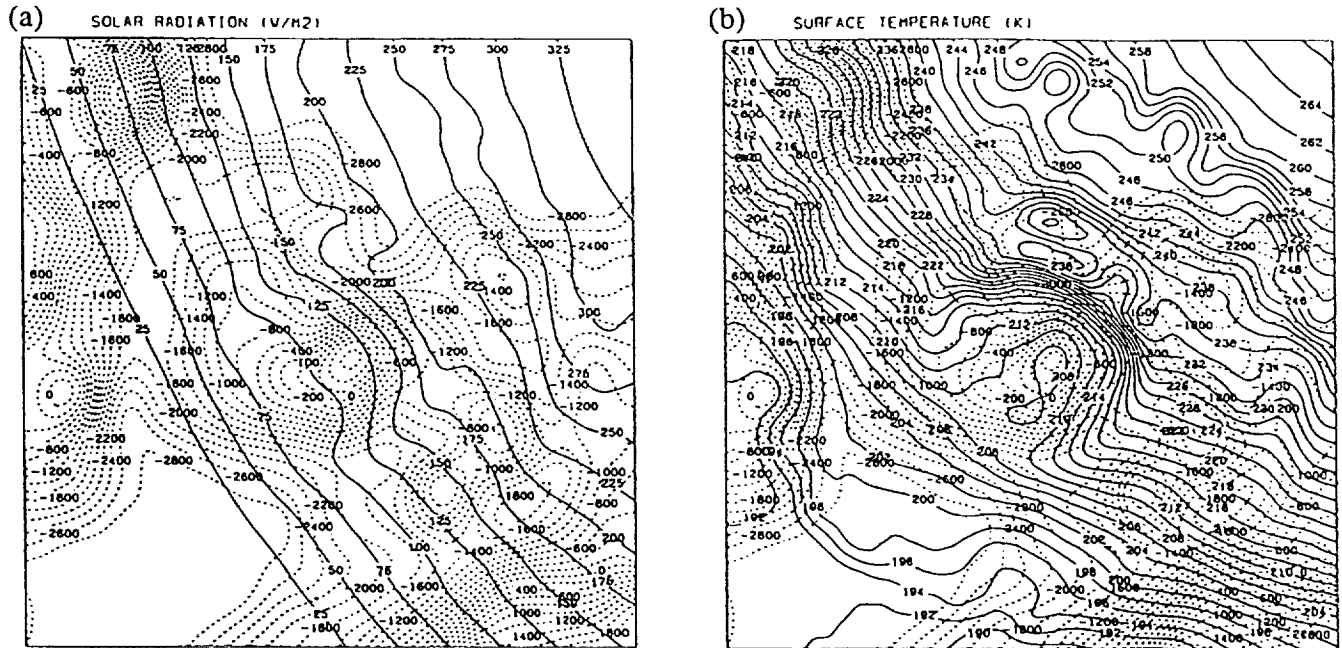


Fig. 3. Intensity of solar radiation ( $\text{W m}^{-2}$ ) (a) reaching the surface and (b) corresponding to surface temperatures from numerical simulation of diurnal cycle over martian north polar cap.

north polar cap. For three-dimensional simulations, terrain heights for the martian north polar region have been obtained from the U.S. Geological Survey map, which have been digitized onto a  $57 \times 57$  grid with a spacing of 75 km.

**Model Results:** *Two-dimensional simulations of thermally induced flows.* A series of numerical experiments have been conducted that focus on the relationship between katabatic wind intensity and terrain slope. The model runs are valid for high-latitude ( $75^\circ$ ), nocturnal conditions similar to midwinter on the north polar cap in which no solar radiation reaches the ground. A horizontal grid consisting of 20 points with a grid spacing of 20 km was used. The results of five 24-hour uniform slope runs are presented here. In each experiment, the model atmosphere was started from rest to isolate the katabatic wind. An initial lapse rate of  $3^\circ\text{C km}^{-1}$  was used with a surface temperature of approximately 220 K at the vertical reference level.

In all cases, the katabatic wind reached a quasisteady state within the first 12 martian hours. The resulting evolution of the wind speed and wind direction at the lowest sigma level (approximately 20 m above the surface) for the five martian katabatic wind simulations after 24 hr are shown in Fig. 1. Curves A–E correspond to terrain slopes of 0.0005, 0.001, 0.002, 0.004, and 0.008 respectively. The intensity of the katabatic wind (Fig. 1a) appears sensitive to the terrain slope. For steeper slopes, the flow remains directed more downslope (downslope direction is  $180^\circ$ ), which implies the horizontal pressure gradient force remains considerably greater than the Coriolis acceleration.

To test the sensitivity of the martian slope flows to solar forcing, numerical experiments have been conducted in which the full cycle of solar forcing is replicated over sloping terrain. Results for a constant slope of 0.008 at  $75^\circ$  latitude will be described.

Five numerical simulations have been conducted covering the seasonal range of solar declination angles ( $24^\circ$ ,  $12^\circ$ ,  $0^\circ$ ,  $-12^\circ$ , and  $-24^\circ$ ); the model equations are integrated for three complete martian days to allow the model to settle into a stable diurnal oscillation. The results presented here are taken from day 2; only minor variations were seen beyond the first diurnal cycle. It is assumed that the polar cap is composed of “dirty” ice with an albedo of 0.50. All simulations start from a rest state. Thus the influence of large-scale pressure gradients in the free atmosphere is neglected. This implies that all atmospheric motions arise due to the longwave radiative cooling or solar heating of the sloping terrain. No solar insolation is allowed for the first 12 hr of model integration time to allow the drainage flows to become established before model sunrise.

Figure 2 illustrates the diurnal course of the surface temperature, wind speed, and wind direction over the 0.008 slope martian terrain for solar declinations of  $24^\circ$ ,  $12^\circ$ ,  $0^\circ$ ,  $-12^\circ$ , and  $-24^\circ$ , corresponding to curves A, B, C, D, and E, respectively. The Sun never sets during the midsummer period and never rises for the winter case. The ground temperature (Fig. 2a) undergoes diurnal oscillations of 30 K in summer; the magnitude of the oscillation decreases with the approach of the autumn; the diurnal ground temperature oscillation amounts to 15 K at the equinox. Maximum temperatures appear an hour or so after local noon. Wind speeds at the first sigma level (Fig. 2b) show marked diurnal trends during summer and equinox periods. Maximum wind speeds occur in the early morning hours coinciding with a minimum in the solar insolation in midsummer or just before sunrise in other simulations. Note that the simulated midsummer katabatic wind maximum of approximately  $10.5 \text{ ms}^{-1}$  (reached in the early morning hours) is  $3 \text{ ms}^{-1}$  less than seen for the other cases. This reflects the insolation from the midnight Sun, which retards development of the katabatic wind. Wind directions

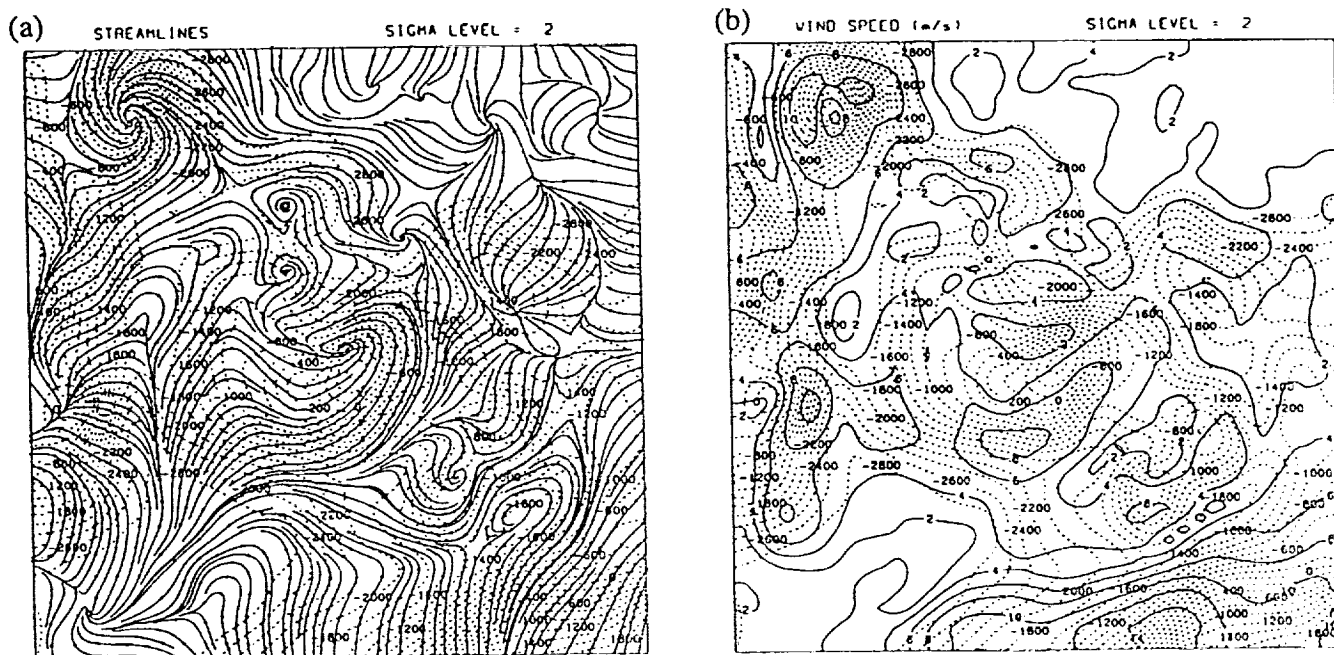


Fig. 4. Model simulations of (a) streamlines and (b) wind speeds of slope flows at the second sigma level for diurnal cycle experiment.

at the first sigma level throughout the diurnal course for the five numerical simulations are shown in Fig. 2c. The downslope direction is  $180^\circ$  for these simulations. The Coriolis force acts to deflect the katabatic wind some  $30^\circ$  to the right of the fall line of the terrain for the winter katabatic wind case. The wind directions show surprisingly little variation with time except for the midsummer declination angle of  $24^\circ$  (curve A). Note that upslope flow is modeled during the early afternoon hours of the summer case. The effect of solar insolation appears to retard but not overcome the katabatic forcing in all but the summertime case. This emphasizes the robust nature of the martian katabatic circulation.

*Three-dimensional simulations of the near-surface flows over the martian north polar cap.* Numerical simulations have also been conducted incorporating solar insolation over the irregular terrain of the northern martian latitudes. For these simulations, the model equations have been integrated for a period of three martian days to ensure that the wind and temperature regimes have had ample time to adjust to the cycle of solar heating. It was found that the second- and third-day results of the model integration were nearly identical. Here the third-day results of one such experiment will be presented. In this experiment, the solar declination is assumed to be  $25^\circ$ , representative of midsummer conditions. It is assumed that the atmosphere is dust-free. As before, the model is initialized about a state of rest to isolate the thermally induced slope flows in the lower atmosphere. Values of albedo and thermal inertia were taken from Paige [9].

Figure 3 illustrates the solar insolation received at the surface and corresponding surface temperatures. Local noon at this time is along the  $60^\circ$  meridian in Fig. 1. Note that significant spatial variations in the intensity of solar radiation reaching the surface are found near the polar cap in response to albedo differences. Surface

temperatures range from 265 K along the southern edge of the domain at local noon to around 190 K in the nighttime section of the model domain.

Anabatic motions become established in response to the solar heating of the sloping terrain. Figure 4 illustrates the streamlines and wind speeds at the second sigma level for the time of the local solar forcing shown in Fig. 3. Note that especially along the local noon meridian, the streamline patterns are dramatically altered by the solar insolation as compared to pure katabatic flow. Upslope wind conditions are simulated at middle to high latitudes from morning through midafternoon. As seen in the previous simulation, the strongest winds are associated with the steepest terrain. Upslope flows reach approximately  $7 \text{ ms}^{-1}$  in places along the local noon meridian. The intensity of the upslope flows appears to be weaker than the nocturnal katabatic winds. This is in agreement with numerous terrestrial observations such as over the Antarctic ice sheet. The katabatic wind speeds simulated over the nighttime sector centered are only slightly weaker than pure katabatic winds (not shown), emphasizing the rapid response of the wind field to the radiative-induced temperature changes near the surface.

**Summary:** Numerical simulations of the martian near-surface wind regime using a mesoscale atmospheric model have shown that the thermally induced near-surface winds are analogous to terrestrial circulations. In particular, katabatic wind displays a striking similarity to flows observed over Antarctica. Introduction of solar radiation strongly perturbs the slope flows; anabatic conditions develop in middle to high latitudes during the daytime hours due to the solar heating of the sloping terrain. There appears to be a rapid transition from the katabatic to the anabatic flow regimes, emphasizing the primary importance of radiative exchanges at the surface in specifying the horizontal pressure gradient force.

- References:** [1] Hess S. L. et al. (1977) *JGR*, 82, 4559–4574. [2] Sutton J. L. et al. *J. Atmos. Sci.*, 35, 2346–2355. [3] Howard A. D. (1981) *NASA TM-82385*, 333–335. [4] Parish T. R. and Waight K. T. (1987) *Mon. Wea. Rev.*, 115, 2214–2226. [5] Anthes R. A. and Warner T. T. (1978) *Mon. Wea. Rev.*, 106, 1045–1078. [6] Brost R. A. and Wyngaard J. C. (1978) *J. Atmos. Sci.*, 35, 1427–1440. [7] Busch N. E. et al. (1976) *J. Appl. Meteor.*, 15, 909–919. [8] Businger J. A. et al. (1971) *J. Atmos. Sci.* 28 181–189 [9] Daise D. A. (1992) *LPS XXIII*, 1013.

**N94-33224**

534.91 ABS. ON  
 APRON HEIGHTS AROUND "STEPPED MASSIFS" IN THE CYDONIA MENSÆ REGION: DO THEY RECORD THE LOCAL PALEOBATHYMETRY OF "OCEANUS BOREALIS"? T. J. Parker and D. S. Gorsline, Department of Geological Sciences, University of Southern California, Los Angeles CA 90089-0740, USA.

Over the past several years a number of investigators have described geomorphic evidence for and paleoclimatic significance of large standing bodies of water or ice sheets within the northern lowland plains of Mars [e.g., 1–14]. The details of the timing, emplacement mechanisms, and sizes of these bodies differ markedly from one group of investigators to another, however. For example, Jöns [1,2] envisioned a "mud ocean" covering much of the northern plains, with sediment slurries derived from a variety of peripheral sources, including the fretted terrains and outflow channels. Lucchitta et al. [4] pictured an ice-covered ocean, fed by large circum-Chryse ice streams, analogous to those in Antarctica. Parker et al. [10,11] indicated two or more highstands of a sea or ocean that, most recently, would have been charged by catastrophic floods, but may have existed more or less permanently during Noachian and Hesperian time. Interestingly, the shorelines of Jöns' "mud ocean," Lucchitta et al.'s ice-covered ocean, and Parker et al.'s most recent sea, or "interior plains" [11], coincide almost precisely around the northern lowlands, though the details of the mechanisms by which key boundary morphologies are thought to have been produced differ. Baker et al. [12] pictured a plainswide ocean emplaced by the major outflow channels relatively late in martian history, and coined the term "Oceanus Borealis" for this ocean.

Taking a more conservative approach to the question of standing water in the northern plains, Rotto and Tanaka [14] have relied on volume estimates of maximum discharge from the circum-Chryse outflow channels, which they feel limits any standing water to one or a few large, ephemeral lakes. The locations of these lakes are based on the identification of broad, shallow topographic basins on the present martian topographic maps [15]. Similarly, Scott et al. [13] have indicated evidence for several large lakes across the northern plains, some exhibiting connecting spillways, that were fed by a variety of channel sources peripheral to the plains. Delineation of these lakes is based on a similar assessment of the topography, but also included the identification of shore morphology.

All the above studies would have benefited greatly from the advent of the high-resolution topography afforded by the Mars Observer Laser Altimeter [16], which would have produced global topographic maps beginning in early 1994. For example, basin volume estimates in Parker et al. [11] are loosely based on the available topography with its very large vertical errors. These estimates, when compared to estimates by others of the water dis-

charged by the Chryse outflow channels, suggest the possibility that the volumes required to fill the basin may be at or beyond the high end of the estimated volumes available from the channels. High-resolution topography is needed to sort out the common modifiers of shoreline elevation, such as tectonism, isostatic rebound, and sediment desiccation and compaction, that probably altered the topography of the northern plains after the putative surface water was lost, so that the original topography can be reconstructed. Until a reflight of the laser altimeter or some similar instrument, elevations derived using the currently available high-resolution topographic tools—photoclinometry and shadow measurements—cannot be accurately tied to the global datum. It is not possible, therefore, to be certain that basin volumes based on the current global topography provide better than a crude approximation of the volume of ancient standing bodies of water in the northern plains. Until they do, such estimates cannot, by themselves, either point to nor preclude the presence of surface water or ice within the northern plains prior to the latest catastrophic floods; the uncertainties are still too large relative to the flood volume estimates.

Can photoclinometry and shadow measurements be used to determine the volume of the basin without having to link the measurements to a global datum? Since the boundary, or shoreline of the basin cannot be tied to the datum and typically has no useful local relative height to measure, what is needed are a number of measurements of the height of the paleoshoreline(s) distributed across the basin—soundings, in effect.

Parker et al. [9,11] described a type of small knob in the northern plains that resembles terrestrial and lunar steppees (volcanic apron) and terrestrial wave-cut islands, and applied the nongenetic term "stepped massifs" to the martian knobs. If these are upland outliers that had been abraded through wave action in an unfrozen ocean, or through ice-shoving in an ice-covered ocean, then the height of the apron above the surrounding plains could provide a measure of the local basin depth in the vicinity of the knob. Since stepped massifs are distributed over broad expanses in several places in the northern plains, it should be possible to measure the variation in basin depth regionally. With the exception of those regions where the available image scale is insufficiently small, it should be possible to measure the heights of the aprons to within a few tens of meters.

As a feasibility test of this approach, photoclinometric profiles are being compiled from Viking Orbiter images of the Cydonia Mensae region, which includes images with high Sun elevations (necessary to avoid shadows) and images with low Sun elevations (to enable the use of shadow measurements as an independent check) at high resolution (40–100 m/pixel). Both asymmetric and symmetric photoclinometric profile models are being used, and the results cross checked with one another to minimize the errors. An apron-height map, potentially a paleobathymetric map of part of the margin of "Oceanus Borealis," will be compiled of this data to determine whether variations in apron height are consistent with a lacustrine interpretation.

- References:** [1] Jöns H.-P. (1985) *LPS XVI*, 414–415. [2] Jöns H.-P. (1986) *LPS XVII*, 404–405. [3] Jöns H.-P. (1990) *Geol. Rundsch.*, 79, 131–164. [4] Lucchitta B. K. et al. (1986) *Proc. LPSC 17th*, in *JGR*, 91, E166–E174. [5] McGill G. E. (1985) *LPS XVI*, 534–535. [6] McGill G. E. (1986) *Geophys. Res. Lett.*, 13, 705–708. [7] McGill G. E. and Hills L. S. (1992) *JGR*, 97, 2633–2647. [8] Parker T. J. et al. (1987) *LPI Tech. Rpt. 87-01*, 96–98. [9] Parker T. J. et al. (1987) *Rept. Planet. Geol. Prog. 1986*, NASA TM-89810,